

**Damped transient response of the giant dipole resonance in the lead region**A. P. Severyukhin,<sup>1,2</sup> S. Åberg,<sup>3</sup> N. N. Arsenyev,<sup>1</sup> and R. G. Nazmitdinov<sup>4,1,2,\*</sup><sup>1</sup>*Bogoliubov Laboratory of Theoretical Physics, Joint Institute for Nuclear Research, 141980 Dubna, Moscow region, Russia*<sup>2</sup>*Dubna State University, 141982 Dubna, Moscow region, Russia*<sup>3</sup>*Mathematical Physics, Lund University, P.O. Box 118, S-22100 Lund, Sweden*<sup>4</sup>*Departament de Física, Universitat de les Illes Balears, E-07122 Palma de Mallorca, Spain*

(Received 21 August 2018; published 25 October 2018)

We analyze thoroughly the statistical properties of the  $1^-$  spectrum in energy interval 9.5–18.5 MeV for  $^{206}\text{Hg}$ ,  $^{204,206,208}\text{Pb}$ , and  $^{210}\text{Po}$  nuclei. To this aim we use the Skyrme interaction SLy4 and the volume pairing interaction, treated in the BCS approximation, as our model Hamiltonian to create a single-particle spectrum and to analyze excited states. The excited states are obtained in the quasiparticle random phase approximation taking into account the coupling between one- and two-phonon states. The obtained spectra (studied by means of the nearest-neighbour spacing distribution,  $\Delta_3$ -statistics and the Porter-Thomas distribution) indicate on the onset of statistical properties close to those of the Gaussian Orthogonal Ensembles. The comparison of the results, obtained with the aid of the coupling calculated microscopically and by means of the Gaussian random distribution, demonstrates a close similarity in the description of the spreading widths of the Isovector Dipole Giant Resonance of the considered nuclei. Furthermore, we show that employing the random distribution for the coupling between microscopic one-phonon states and two-phonon states, generated by the Gaussian Orthogonal Ensembles distribution, a good agreement is also obtained with the microscopic description of the decay widths.

DOI: [10.1103/PhysRevC.98.044319](https://doi.org/10.1103/PhysRevC.98.044319)**I. INTRODUCTION**

Many spectral properties of doubly magic nuclei  $^{208}\text{Pb}$  are relatively well understood in terms of nuclear shell model. A number of high-resolution experiments demonstrate, however, that fluctuation properties of energy spectra of  $^{208}\text{Pb}$  could be interpreted as well in terms of the Random Matrix Theory (RMT). In particular, recent analysis of 151 experimental nuclear levels up to excitation energy of  $E_x = 6.2$  MeV in  $^{208}\text{Pb}$  indicates that the spectral properties are described already by the Gaussian orthogonal ensembles (GOE), even though there is a small admixture of regular dynamics brought about by the low-lying states (e.g., Refs. [1,2]). We recall that, nowadays, the RMT is a well established theoretical approach [3], often used for analysis of regular and chaotic aspects of nuclear structure (e.g., Refs. [4–9]).

Naturally, one would expect that chaotic component of intrinsic structure of a finite many-body quantum system, exhibited in its spectral properties at low excitation energy, may transform from the secondary constituent to the dominant one in basic characteristics of the considered system with increase of the excitation energy. This might be primarily true in the description of radiative decay of nuclear giant resonances (GRs), highly excited collective states which centroids are located above the neutron threshold [10]. From this point of view, the isovector giant dipole resonance (IVGDR), for example, in  $^{208}\text{Pb}$ , i.e., the most studied case (e.g., Refs. [11–14], to name just a few), provides a prosperous

platform for study of chaotic and regular features of heavy nuclei.

Indeed, on the one hand, the IVGDR is essentially excited by an external field through a one-body interaction. It is, therefore, natural to describe such a mode as a collective one-particle-one-hole (1p-1h) state. Its centroid is empirically given by  $E_c \approx 31.2A^{-1/3} + 20.6A^{-1/6}$  [15]. On the other hand, in general, once excited, the GR progresses to a fully equilibrated system via direct particle emission and by coupling to more complicated configurations (2p-2h, 3p-3h, etc.). In other words, the wave function of this collective mode is not an eigenstate of the nuclear Hamiltonian, but it rather spreads over many eigenstates that are characterized by the same quantum numbers such as the angular momentum and the parity:  $J^\pi = 1^-$ . The former mechanism gives rise to an escape width ( $\Gamma^\uparrow$ ). It is expected that the decay evolution along the hierarchy of more complex configurations to compound states determines a spreading width ( $\Gamma^\downarrow$ ). Together, with Landau damping ( $\Gamma_L$ ), the above-mentioned components form the decay width  $\Gamma = \Gamma^\downarrow + \Gamma^\uparrow + \Gamma_L$ . It would be of undoubted interest to answer the question: how important are chaotic constituents for the formation of the decay width of the IVGDR in  $^{208}\text{Pb}$  and nuclei of its closed neighborhood?

Conceptually, a description of the decay width represents a fundamental problem which is, however, difficult to solve due to the existence of many degrees of freedom for many-body quantum system. As a rule, the escape width ( $\Gamma^\uparrow$ ) is not included in any calculation with a discrete basis. While the description of spreading width in mesoscopic systems is based on the study of the electromagnetic strength distribution (strength function) [16] in some energy interval. This interval

\*rashid@theor.jinr.ru

should be large enough to catch hold of basic features of a GR under investigation. Note that in deformed quantum many-body systems the experimental widths are systematically larger and may develop a two- or three-peak structure. In this paper we consider only spherical or near-spherical nuclei around  $^{208}\text{Pb}$ . Consequently, we remove additional effects due to deformation to highlight a generic nature of the decay width  $\Gamma \approx \Gamma^\downarrow + \Gamma_L$  of the IVGDR in heavy nuclei.

To gain an insight into fragmentation of high-lying states over complex configurations, observed as the IVGDR spreading, we have to introduce various approximations or a realistic nuclear structure model, which validity depends on a primal feasibility. It should be based on the microscopic many-body theory, where the effects of the residual interaction on the statistics must be studied in a large model space. In particular, the description of a near-spherical nucleus requires the consideration of pairing forces. Although these forces increase drastically the model configuration space, an enlarged set of corresponding states provide favourable conditions for applications of the RMT. Note that among other things, introducing a residual interaction in general implies a transition to the GOE-properties above some excitation energy [17,18].

Nuclear shell model may be used to analyze spreading widths of GRs. However, the complexity of the calculations increases rapidly with the size of the configuration space. This fact severely restricts the feasibility of shell model calculations for heavy and super-heavy nuclei. In addition, even for a medium  $^{48}\text{Ca}$  isotope the state-of-art shell model calculations [19], which operate with the Hamiltonian matrices of a huge dimension, produce questionable results for the dipole GR. Although these calculations reproduce reasonably well its peak position and peak width, the enhancement of the classical Thomas-Reiche-Kuhn (TRK) sum rules is too overestimated. As a result, the number of shell model studies, in particular, dipole GRs in heavy and super-heavy nuclei are limited and rather focused on details of the low-energy region (e.g., Ref. [20]).

The quasiparticle-phonon model (QPM) [21] offers an attractive framework for such studies. We will use the modern development of the QPM, a finite rank separable approximation (FRSA) [22,23]. That approach employs the Skyrme forces to calculate the single-particle spectrum and the residual interaction in a self-consistent manner to avoid any artefacts [24]. We will discuss the FRSA in some details in Sec. II.

The success of the RMT, based on universal features in spectra of complex quantum systems (e.g., Refs. [25–27]), gives hope to shed light on the spectral properties and the distribution of transition-strength properties of the IVGDR, when specific details become not of a primary importance. As is well known, the RMT assumes only that a many-body Hamiltonian belongs to an ensemble of random matrices that are consistent with the fundamental symmetries of the system such as parity, rotational, translational and time-reversal symmetries. We believe that it is quite suitable for our main goal which is to answer to the basic question: Could the RMT provide a practical and useful recipe for description of the IVGDR decay? To proceed, we analyze first spectral properties of the IVGDR within the RMT in Sec. III.

Some limiting analytical estimates for the IVGDR strength function were obtained by considering the random coupling of one structureless doorway state to chaotic background [28,29]. Evidently, the extension of the wave function to more complex configurations might increase the fragmentation of the one-phonon strength over many excited states (see discussion in Ref. [30]). Although it would allow to discuss fine structure of GRs, it shall require more cumbersome numerical calculations, without crucial insight to our analysis focused on their gross structures. In our preliminary studies [31] we have shown that the microscopic phonon-phonon coupling (PPC) [i.e., the microscopic matrix elements  $V_{2\text{ph}}^{1\text{ph}}$  between the one-phonon (1ph) and the two-phonon (2ph) configurations] describes reasonably well the gross structure of spreading widths of giant monopole, dipole, and quadrupole resonances in the doubly magic heavy nuclei. Further, in the form of the random coupling of the one-phonon with the two-phonon states, gross structure of the strength distributions of giant multipole resonances are obtained and have been compared with the microscopic PPC results. Therefore, we named our approach as the damped transient response.

The basic idea of our approach (to use the random coupling) raised, however, doubts about its fairness [32]. We demonstrated evidently in Ref. [33] that the Comment [32] fails to provide plausible arguments against the description of the gross structure with the aid of the random matrix theory. Below we will discuss all pros and cons of our approach, focusing only on the decay width of the IVGDR in the lead region. We will also present the description of these widths in terms of a simple random matrix model, comparing the results with the microscopic ones in Sec. IV. Summary will be given in Sec. V.

## II. BASIC ELEMENTS OF THE MICROSCOPIC APPROACH

### A. Mean field

The starting point of our microscopic approach consists in the Hartree-Fock (HF)+BCS calculation of the ground state based on the Skyrme energy density functional (EDF) [34]. Spherical symmetry is imposed on the quasiparticle wave functions. The continuous part of the single-particle spectrum is discretized (see details in Ref. [35]) by diagonalizing the Skyrme HF Hamiltonian on a basis of 12 harmonic oscillator shells. We use the SLy4 EDF [36] in the p-h channel. The parameters of the SLy4 EDF have been adjusted to reproduce nuclear matter properties, as well as nuclear charge radii, binding energies of doubly magic nuclei.

The pairing correlations are generated with the aid of a density-dependent zero-range force,

$$V_{\text{pair}}(\mathbf{r}_1, \mathbf{r}_2) = V_0 \left[ 1 - \eta \frac{\rho(r_1)}{\rho_0} \right] \delta(\mathbf{r}_1 - \mathbf{r}_2), \quad (1)$$

where  $\rho(r_1)$  is the particle density in a coordinate space, with  $\rho_0$  being the nuclear matter saturation density. Here, the parameters  $\eta = 0$  and  $\eta = 1$  correspond to a volume interaction and a surface-peaked interaction, respectively. To limit the pairing single-particle space, we have used the smooth cutoff

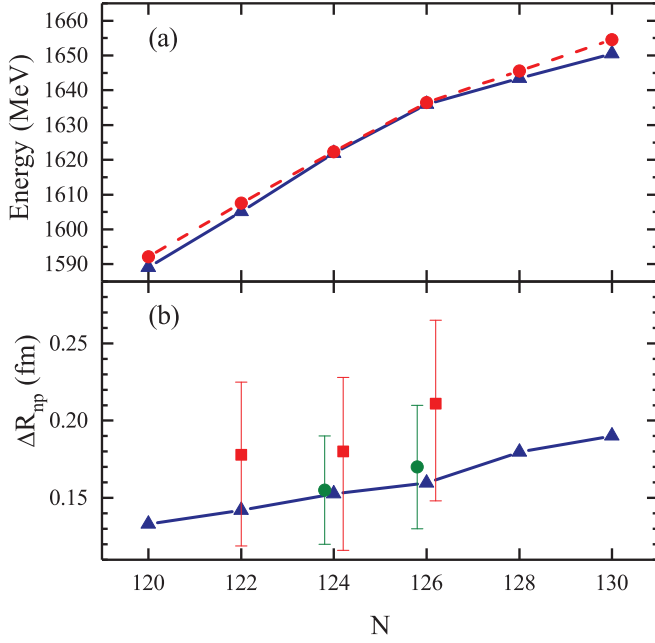


FIG. 1. (a) Binding energies of the even-even Pb isotopes as a function of neutron number, compared with experiment and extrapolated energies (filled circles) from the AME2016 atomic mass evaluation [39]. Results of the calculations within the HF+BCS with the SLy4 EDF are shown by filled triangles. (b) The neutron skin thickness  $\Delta R_{np}$  of the Pb isotopes calculated within the same approach (filled triangles). Experimental data of the neutron skin thickness are taken from the analysis of: (i) proton elastic scattering at 295 MeV [40] (filled squares); (ii) the  $E1$  strength distribution [41] (filled circles).

at 10 MeV above the Fermi energies [23,37,38]. The strength  $V_0 = -280 \text{ MeV fm}^3$ , taken at  $\eta = 0$ , is fitted to reproduce the experimental pairing gaps of  $^{206}\text{Hg}$ ,  $^{206}\text{Pb}$ , and  $^{210}\text{Po}$  obtained by means of the three-point formula [23].

The HF+BCS with the SLy4 EDF describes correctly the binding energies of even-even Pb isotopes [see Fig. 1(a)]. Indeed, the results of calculations and experimental data for  $^{202-212}\text{Pb}$  are in a good agreement, the deviations being less than 0.2%.

We also compare the calculated neutron skin thickness  $\Delta R_{np}$ , defined as

$$\Delta R_{np} = \sqrt{\langle r^2 \rangle_n} - \sqrt{\langle r^2 \rangle_p}, \quad (2)$$

with the experimental data for  $^{204,206,208}\text{Pb}$  [see Fig. 1(b)]. The proton-neutron root-mean square (rms) differences become larger with the increase of the neutron number. The available experimental data are reasonably well reproduced. In the case of  $^{208}\text{Pb}$ , the theoretical “model-averaged” estimate for  $\Delta R_{np}$  is  $0.168 \pm 0.022 \text{ fm}$  [42].

### B. Configuration mixing of collective states

The residual particle-hole interaction is obtained as the second derivative of the EDF with respect to the particle density. Namely, the residual interaction in the p-h channel

is consistently derived from the Skyrme forces, while the residual interaction in the particle-particle (p-p) channel is obtained from the zero-range pairing forces [43].

By means of the standard procedure [34] we obtain the familiar equations of the quasiparticle random phase approximation (QRPA). The cutoff of the discretized continuous part of the single-particle spectra is taken at the energy of 100 MeV. This is sufficient to exhaust practically all the sum rules. The eigenvalues of the QRPA equations are found numerically as the roots of a relatively simple secular equation within the FRSA [22,23]. The QRPA solutions are treated as quasi-bosons with quantum numbers  $\lambda^\pi$ . Among these solutions there are one-phonon states  $\omega_{\lambda i}$  corresponding to collective GRs and pure two-quasiparticle states.

Using the basic QPM ideas in the simplest case of the configuration mixing [21], we construct the wave functions from a linear combination of one-phonon and two-phonon configurations states as

$$\Psi_\nu(\lambda\mu) = \left\{ \sum_i R_i(\lambda\nu) Q_{\lambda\mu}^+ + \sum_{\lambda_1 i_1 \lambda_2 i_2} P_{\lambda_2 i_2}^{\lambda_1 i_1}(\lambda\nu) [Q_{\lambda_1 \mu_1 i_1}^+ Q_{\lambda_2 \mu_2 i_2}^+]_{\lambda\mu} \right\} |0\rangle, \quad (3)$$

where  $\lambda$  denotes the total angular momentum and  $\mu$  its  $z$ -projection in the laboratory system. The ground state is the QRPA phonon vacuum  $|0\rangle$ . The unknown amplitudes  $R_i(\lambda\nu)$  and  $P_{\lambda_2 i_2}^{\lambda_1 i_1}(\lambda\nu)$  are determined from the variational principle, which leads to a set of linear equations [44,45]

$$(\omega_{\lambda i} - E_\nu) R_i(\lambda\nu) + \sum_{\lambda_1 i_1 \lambda_2 i_2} U_{\lambda_2 i_2}^{\lambda_1 i_1}(\lambda i) P_{\lambda_2 i_2}^{\lambda_1 i_1}(\lambda\nu) = 0, \quad (4)$$

$$\sum_i U_{\lambda_2 i_2}^{\lambda_1 i_1}(\lambda i) R_i(\lambda\nu) + 2(\omega_{\lambda_1 i_1} + \omega_{\lambda_2 i_2} - E_\nu) P_{\lambda_2 i_2}^{\lambda_1 i_1}(\lambda\nu) = 0. \quad (5)$$

The rank of the set of linear Eqs. (4) and (5) is equal to the number of one- and two-phonon configurations included in the wave function Eq. (3). Its solution requires computing the Hamiltonian matrix elements of the coupling between one- and two-phonon configurations:

$$U_{\lambda_2 i_2}^{\lambda_1 i_1}(\lambda i) = \langle 0 | Q_{\lambda i} H [Q_{\lambda_1 i_1}^+ Q_{\lambda_2 i_2}^+]_{\lambda} | 0 \rangle. \quad (6)$$

Our approach is similar to the particle-vibration coupling (PVC) model based on Green’s function method (see for a recent review Ref. [46]) that has been used in the study of the monopole [47] and the quadrupole [48] GR widths in  $^{208}\text{Pb}$  with the aid of the Skyrme forces. Note that the PPC includes as well the coupling of one-phonon state with two-particle two-hole states (important in the PVC model) as a particular case (see Ref. [49] and discussion in Chapter 4.3 of the textbook [21]). However, a consistent realization of the QPM as well as the PVC model (which closely follows the concept of the “conserving approximation” introduced by Baym and Kadanoff [50]) is very difficult to implement numerically. In particular, to let the two-phonon components

of the wave functions Eq. (3) obey the Pauli principle the exact commutation relations between the phonon operators should be taken into account [21]. As a result, this would lead to the “dressed” two-phonon energies, here not accounted for. As we will see below, the random matrix approach enables us to avoid this problem effectively.

To construct the wave functions Eq. (3) of the  $1^-$  states, in the present study we take into account all two-phonon terms that are built from the phonons with different multipoles  $\lambda^\pi = 0^+, 1^-, 2^+, 3^-, 4^+$  coupled to  $1^-$ . Tentative estimates for the position of the resonance centroids  $E_c$  and the spreading width  $\Gamma$  are defined by means of the energy-weighted moments  $m_k = \sum B(E\lambda) E^k$ : (i)  $E_c = m_1/m_0$ ; (ii)  $\Gamma = 2.35\sqrt{m_2/m_0 - (m_1/m_0)^2}$  (see, for example, Ref. [51]). Note that the coefficient 2.35 has its roots to the experimental definition of the width (full width at half maximum) related to the variance of the Gaussian (see, for example, Ref. [52]).

One of the basic ingredients for the fitting protocol of the SLy4 EDF is the enhancement factor of the TRK sum rule:  $1 + \kappa = 1.25$ . Taking into account this fact, we construct various combinations of two-phonon states  $\omega_{\lambda_1 i_1} + \omega_{\lambda_2 i_2}$  to define the energy interval for location of the resonance width of fixed quantum number  $\lambda^\pi$ , taking 95% of the energy-weighted sum rule symmetrically around the centroid’s position ( $E_c$ ). It is noteworthy that for all the  $E1$  distributions, considered in the present paper, the matrix elements for direct excitation of two-phonon components from the ground state are about two orders of magnitude smaller relative to ones for the excitation of one-phonon configurations. However, the density of these complex configurations is much higher than the one-phonon density, and contributes essentially to statistics of the final states.

We start our discussion of the spreading width of the IVDGR, recapitulating our results for the spherical  $^{208}\text{Pb}$  nucleus [31]. We recall, that the  $(\Gamma^\dagger)$  width is not included in any calculation of giant resonances with a discrete basis. To mimic the missed mechanisms and to compare different results, we use a typical for various calculations smoothing parameter value 1 MeV (e.g., Refs. [53–56]) to calculate the strength distribution with the aid of the Lorentzian smearing. The coupling (the PPC) of the one-phonon states with an intermediate complex background of the two-phonon states yields a strong redistribution of the one-phonon dipole strength in the region of the IVDGR (see Fig. 1(c) in Ref. [31]). It suppresses the high-lying one-phonon strength near 17 MeV and pushes this strength down (see also Ref. [11]). As a result, we obtain a reasonably well description of the dipole strength distribution over the resonance localization region (compare Figs. 1(a) and 1(b) in Ref. [31]). It appears that the presence of the two-phonon components in our wave function, in addition to the one-phonon ones, already enables us to describe the gross strength distribution of the typical dipole response in the heavy spherical nucleus  $^{208}\text{Pb}$ . Similar conclusions have been drawn on the basis of shell-model calculations for the states above 8 MeV in Ref. [20].

To test further the validity of our microscopic approach we compare the results of the  $E1$  strength distributions,

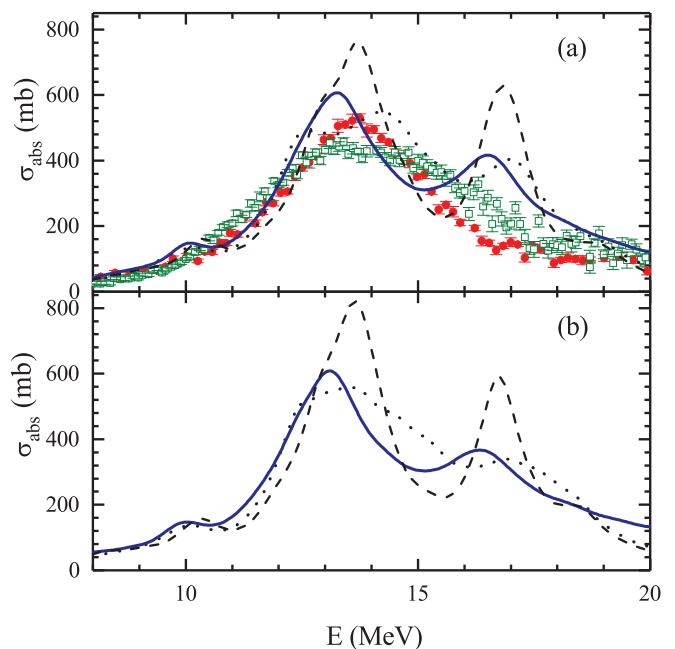


FIG. 2. Photoabsorption cross section ( $\sigma_{\text{abs}}$ ) for  $^{206}\text{Pb}$  (a) and  $^{206}\text{Hg}$  (b). The experimental photoabsorption cross section for  $^{206}\text{Pb}$  deduced from Ref. [57] (filled circles) and from Ref. [58] (open squares). The dotted and solid lines correspond to the results obtained by means of the microscopic and the random coupling matrix elements between the one- and two-phonon configurations, respectively. The dashed line connects the QRPA (one-phonon) results. The smoothing parameter 1 MeV is used for the strength distribution described by the Lorentzian function.

obtained by means of the PPC (when the neutron pairing is taken into account), with experimental data available for  $^{206}\text{Pb}$  [see Fig. 2(a)]. The photoabsorption process is well studied experimentally in this case (e.g., Refs. [57,58]). We find that the total energy-weighted  $E1$  strength calculated in the QRPA with the SLy4 EDF exhausts 92.8% of the TRK sum rule value in the energy region 9.5–18.5 MeV. The inclusion of the two-phonon terms results in the decrease of the integrated energy-weighted  $E1$  strength by 0.8%. The PPC increases the decay width from 4.6 MeV to 4.9 MeV. The IVGDR shapes obtained by means of the PPC are rather close to those observed in experiment.

Keeping in mind the feasibility of experimental study of the IVGDR in the considered region, we calculate also the strength distribution in  $^{206}\text{Hg}$ ,  $^{204,206,208}\text{Pb}$ , and  $^{210}\text{Po}$  nuclei (see Table I). For the sake of illustration, the strength distribution in  $^{206}\text{Hg}$ , where proton pairing is switched on, is shown on Fig. 2(b). We found very close correspondence in the dipole response, when the pairing channel switched from neutron to proton constituent (see Fig. 2). In general, although the PPC affects the strength distribution in all considered nuclei (see Table I), the difference between the RPA and the PPC results is of order  $\sim 5\%$  for the decay widths. It appears that in the considered cases the basic mechanism of the decay widths is Landau damping, while the PPC (spreading) produces the visible redistribution.

TABLE I. Characteristics of the GDR for  $^{206}\text{Hg}$ ,  $^{204,206,208}\text{Pb}$ , and  $^{210}\text{Po}$  nuclei: centroid energies  $E_c$  and the spreading widths  $\Gamma$  calculated with the QRPA and QRPA plus phonon-phonon coupling with the microscopic (PPC) and random distribution of coupling matrix elements (Random) are compared with available experimental data [15,57]. The values of  $E_c$  and  $\Gamma$  have been computed in the energy region 9.5–18.5 MeV. For comparison the centroid energy and width values from the empirical systematics (Syst.) are presented [15,59].

	$E_c$ (MeV)					$\Gamma$ (MeV)				
	Expt.	Syst.	QRPA	Theory PPC	Random	Expt.	Syst.	QRPA	Theory PPC	Random
$^{206}\text{Hg}$		13.76	14.1	14.1	13.8		4.16	4.6	5.0	5.0
$^{204}\text{Pb}$		13.79	14.3	14.3	14.1		4.17	4.7	4.8	4.9
$^{206}\text{Pb}$	13.59 13.7	13.76	14.2	14.1	14.0	3.85 3.75	4.16	4.6	4.9	4.9
$^{208}\text{Pb}$	13.43 13.6	13.73	14.0	14.0	13.8	4.07 3.78	4.15	4.6	4.9	4.8
$^{210}\text{Po}$		13.70	14.2	14.1	13.9		4.15	4.7	4.9	5.0

### III. SPECTRAL STATISTICS

To elucidate a question of the statistical relationship among regular and chaotic constituents in the  $1^-$  spectra, obtained within our model, we employ two typical RMT measures: the nearest-neighbor spacing distribution (NNSD) and spectral rigidity of Dyson and Metha, the  $\Delta_3$  statistics [60]. The RMT enables us to study the statistical laws governing fluctuations that, in general, can have very different origins.

For a regular system the probability for the NNSD is known as the Poisson distribution,

$$P(s) = e^{-s}. \quad (7)$$

Here, the spacing  $s_i = x_{i+1} - x_i$  is defined for the unfolded spectrum obtained by the mapping  $x_i = S(E_i)$  (see details in Ref. [61]). For a classically chaotic system, that quantum-mechanically is described by the GOE [62], the NNSD is approximately given by the Wigner surmise

$$P(s) = (\pi/2)s \exp[-\pi s^2/4]. \quad (8)$$

In practical calculations  $\bar{\Delta}_3(L)$  can be easily calculated from the number statistics,  $n(L)$ , which is the number of levels in an energy interval of length  $L$ ,

$$\bar{\Delta}_3(L) = \frac{2}{L^4} \int_0^L (L^3 - 2L^2r + r^3) \Sigma^2(r) dr, \quad (9)$$

where

$$\Sigma^2(r) = \langle [n(r) - \langle n(r) \rangle]^2 \rangle \quad (10)$$

is the second moment of  $n(L)$ , and  $\langle n(r) \rangle = r$ . For an uncorrelated spectrum one has

$$\bar{\Delta}_3(L) = L/15, \quad (11)$$

while for the GOE it is

$$\bar{\Delta}_3(L) \approx \frac{1}{\pi^2} (\ln L - 0.0687), \quad (12)$$

in the  $L \gg 1$  limit.

The analysis of the PPC results for the  $^{204,206,208}\text{Pb}$  isotopes exhibits properties inbetween regularity and chaos for the

NNSD [see Figs. 3(a), 3(d) and 3(g)] for all nuclei. Similar result is observed for the  $\bar{\Delta}_3$  statistics. Alike behavior is also found for  $N=82$  isotones [see Figs. 4(a), 4(b) 4(d), and 4(e)]. It appears that the microscopic coupling between the one- and two-phonon components indicates only the basic trend towards the GOE limit in the spectral properties. It is expected, however, that the inclusion of higher complexity configurations would manifest the growth of randomness of spectral properties. Evidently, the latter procedure will increase the density of states that will enforce the statistical properties. We will return to this point in Sec. IV.

Another useful signature of chaos is the statistical fluctuations of the  $B(E1)$ -transition intensities that probe the system's wave functions (see, e.g., Ref. [63] and references therein). To study the fluctuation properties of the transition rates, it is necessary to divide out any secular variation of the average strength function versus the energy. For that purpose we define an average intensity

$$\bar{y}(x_k) = \frac{\sum_n B(E1; 0_{\text{gs}}^+ \rightarrow 1_n^-; x_n) \exp[-(x_k - x_n)^2]/2\gamma^2}{\sum_n \exp[-(x_k - x_n)^2]/2\gamma^2} \quad (13)$$

around the corresponding unfolded energy  $x_k$ . The Gaussian width  $\gamma$  should be chosen properly [64]. In the present calculations we use  $\gamma = 2.0$ .

We renormalize the actual intensities by dividing out their smooth part,

$$y(x_k) = B(E1; 0_{\text{gs}}^+ \rightarrow 1_k^-; x_k) / \bar{y}(x_k), \quad (14)$$

and we construct their distribution using bins that are equally spaced in  $\log_{10} y$ . The choice of  $\log_{10} y$  as the variable allows us to display the distribution of the weak transitions over several orders of magnitude [65]. The magnitude of  $y$  will differ for different final states and, hence, one can construct the density function,  $P(y)$ , of  $y$  such that  $P(y)dy$  is the probability to locate the transition strength in the interval  $dy$  around  $y$ . Then, the interpolating function for  $P(y)$  is a  $\chi^2$

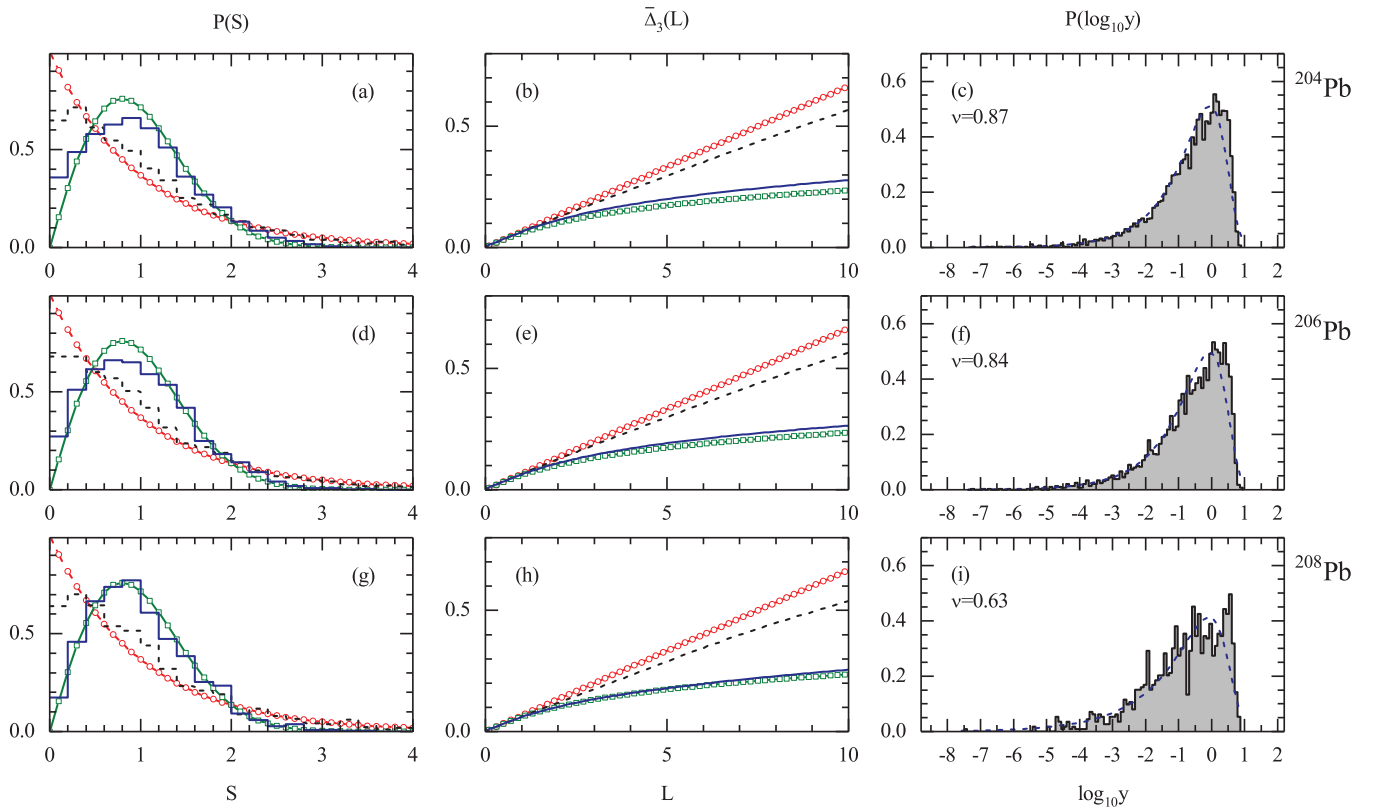


FIG. 3. Spectral and  $B(E1)$  intensity fluctuations for the  $^{204,206,208}\text{Pb}$  isotopes. Left column: the nearest-neighbor spacing distribution  $P(S)$ . Middle column: the  $\bar{\Delta}_3(L)$  statistics of the Dyson and Metha. Right column: the  $B(E1)$  intensity distribution  $P(\log_{10} y)$  where the dashed lines are the fit to  $\chi^2$  distributions with the quoted  $\nu$  degrees of freedom. In the left and middle columns the solid-circle lines describe the Poisson statistics and the solid-square lines are the GOE limit. The dashed and solid lines correspond to the results obtained by means of the microscopic and the random coupling matrix elements between the one- and two-phonon configurations, respectively.

distribution in  $\nu$  degrees of freedom [65]:

$$P_\nu(y) = \frac{1}{y} \left( \frac{\nu y}{2\langle y \rangle} \right)^{\nu/2} \frac{\exp[-\nu y/2\langle y \rangle]}{\Gamma(\nu/2)}, \quad (15)$$

and is fitted to the histogram, through a least squares fitting, to find the best value of  $\nu$ . When  $\nu = 1$ , the interpolating function reduces to the Porter-Thomas distribution [66], which is

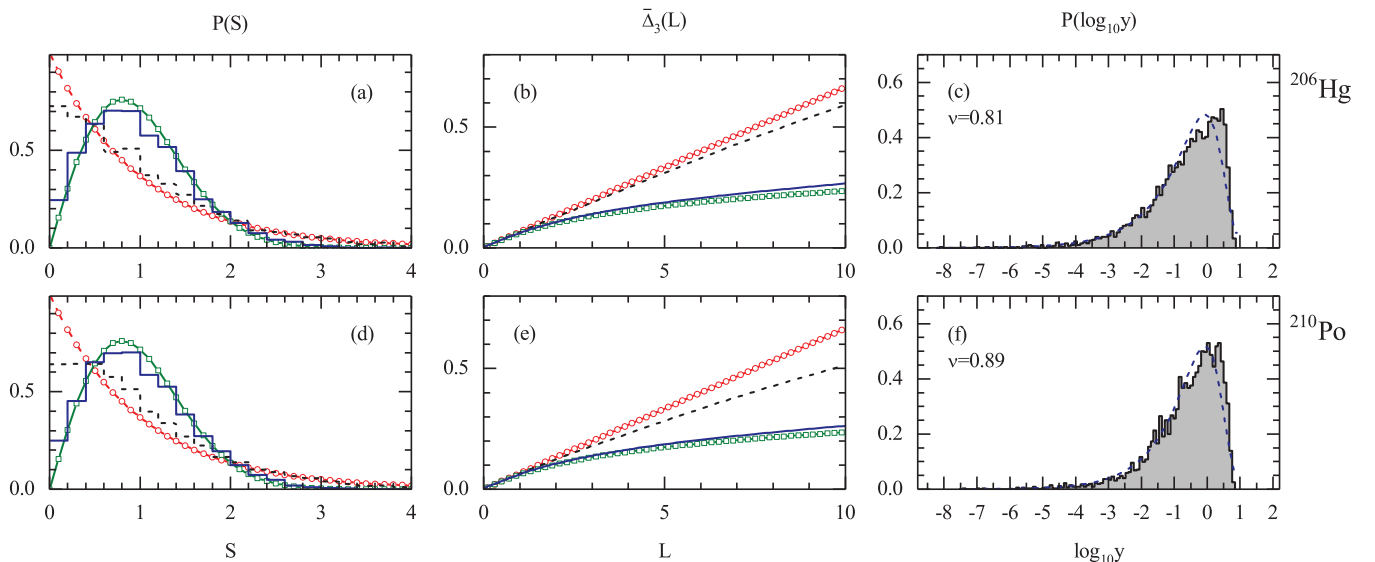


FIG. 4. Similar to Fig. 3, for  $^{206}\text{Hg}$  and  $^{210}\text{Po}$ .

the GOE limit

$$P_{\nu=1}(y) = \frac{1}{\sqrt{y}} \left( \frac{1}{2\pi\langle y \rangle} \right)^{1/2} \exp[-y/2\langle y \rangle], \quad (16)$$

while small  $\nu$ -values are expected for a regular system.

The analysis of the PPC results for the  $^{204,206,208}\text{Pb}$  isotopes exhibits the transition from regular to chaotic features [see Figs. 3(c), 3(f) and 3(i)] with the decrease of the neutron number. Surprisingly, the statistical fluctuations of the  $B(E1)$ -transition intensities (that probe the system's wave functions) indicate on the strong presence of chaotic components. The  $B(E1)$  strength distributions for the  $^{204,206}\text{Pb}$  isotopes alike to those for the  $N = 82$  isotones [compare Figs. 3(c) and 3(f) with Figs. 4(c) and 4(f)]. In these cases the distribution is close to the GOE limit. Note, however, that for the closed-shell nucleus  $^{208}\text{Pb}$  the  $B(E1)$  distribution manifests less degree of chaoticity, which might be related to less degree of statistics. Indeed, the inclusion of the pairing correlations increases the density of states for the open-shell nuclei, which affects the statistical properties.

Summarizing, we notice that the traditional spectral correlations indicate only on a weak blow-up GOE regime within the considered microscopic model. In other words, the coupling of the one- and two-phonon components not allows to make an unambiguous conclusion on the dominance of chaotic features in spectral properties of the IVGDR in heavy nuclei around  $^{208}\text{Pb}$ . It is rather a soft chaotic behavior, which is partially due to insufficient statistics. However, the wave function analysis indicates on the dominance of the chaotic properties in the strength distribution of the dipole transitions.

Could we conclude that the RMT would be uninformative for the description of the spreading width in this situation? The answer on this question is addressed in the next section.

#### IV. RANDOM MATRIX TREATMENT OF THE FRAGMENTATION STRENGTH

We recall that the QRPA calculations imply a fragmentation of the IVGDR strength on several one-phonon states (Landau damping). While the PPC given by Eq. (6) provides the increase in the fragmentation of the strength. As it was mentioned above, in principle, the coupling might include more complicated states, three-phonon states, four-phonon states, etc., with an increasing computational difficulty. Since the IVGDR strength appears at high excitation energies (around 14 MeV for nuclei in the lead region), the considered one- and two-phonon states are surrounded by a large amount of states, that are of the type  $n$ -phonon states with  $n > 2$ . Including the coupling to these complex states is expected to produce a chaotic mixing, since the IVGDR centroids are in an energy region far beyond the location of neutron resonances (e.g., Refs. [4,8]). In this region energies and matrix elements are found to fluctuate obeying rather the GOE-statistics. This motivates a statistical description of the IVGDR fragmentation using ideas from the RMT, as was briefly described in Ref. [31]. We utilize the microscopic calculations of the one-phonon states while the coupling matrix elements between the one-phonon and two-phonon states are replaced by random matrix elements of the GOE-type.

The one-phonon states are thus considered as doorway states to the fragmentation of  $E1$ -strength on background states. Thus, our aim is to describe microscopically the one-phonon IVGDR states, and attempt a random matrix inspired treatment of the coupling to complex surrounding states, here viewed as two-phonon states. The quality of the random treatment can then be studied by comparing results with the microscopic PPC model predictions.

In Sec. IV A the model is presented, and in Sec. IV B we describe how the coupling strength is determined. An alternative way to generate the two-phonon (background) energies is to assume the GOE distributed states, as is discussed in Sec. IV C.

##### A. Doorway model for the fragmentation

Let us describe the IVGDR coupling to various background and ground states by a doorway Hamiltonian (cf. Refs. [16,31]),

$$H = H_d + H_b + V, \quad (17)$$

Here, the Hamiltonian

$$H_d = \sum_i^{N_d} \omega_i Q_i^+ Q_i, \quad (18)$$

is characterized by energies  $\omega_i$  obtained from the microscopic QRPA-calculations of the dipole phonon states, and the  $N_d$  one-phonon states constitute the doorway states. Corresponding eigenstates are  $|d; \omega_i\rangle$ . Transition matrix elements between the ground state and the one-phonon state are obtained from the QRPA calculation as

$$B_i = \langle d; \omega_i | \mathcal{M}_{1^-} | 0 \rangle, \quad (19)$$

where  $|0\rangle$  is the QRPA ground state, and  $\mathcal{M}_{1^-}$  is the  $E1$  dipole operator for  $1^-$  transitions.

The  $N_b$  background states are described by the Hamiltonian

$$H_b = \sum_k^{N_b} \Omega_k a_k^+ a_k, \quad (20)$$

with eigenstates  $|b; \Omega_k\rangle$  and corresponding energies  $\Omega_k$ . The number of background states is much larger than the number of doorway states,  $N_b \gg N_d$ . The  $E1$  matrix element between the ground state and all background states is zero,

$$0 = \langle b; \Omega_k | \mathcal{M}_{1^-} | 0 \rangle. \quad (21)$$

We shall investigate two different ways to obtain the energies  $\Omega_k$ , corresponding to two levels of approximation in setting up our random matrix model:

- (1) The two-phonon states are obtained by coupling the angular momenta of two one-phonon states to a  $1^-$  states,  $[Q_{\lambda_1}^+ Q_{\lambda_2}^+]_{1^-}$ . Each one-phonon state is microscopically calculated in the QRPA model, with energies  $\omega_{\lambda_1}$  and  $\omega_{\lambda_2}$ , respectively, and the energies of the background state is then  $\Omega_k = \omega_{\lambda_1} + \omega_{\lambda_2}$ .
- (2) A higher level of approximation is also considered in this paper, where the background states are randomly

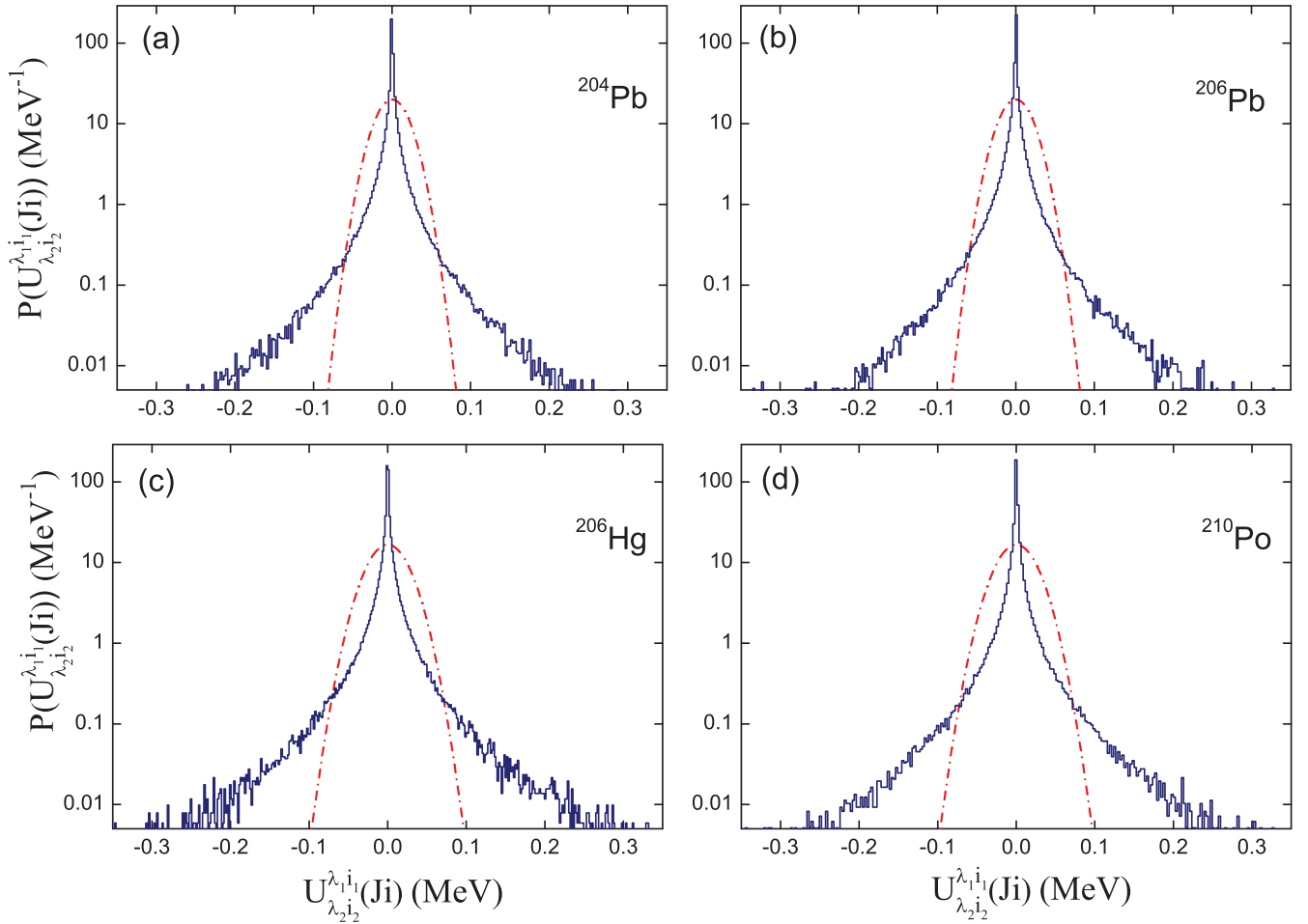


FIG. 5. Distribution of coupling matrix elements between the one- and two-phonon QRPA configurations for  $^{206}\text{Hg}$ ,  $^{204,206}\text{Pb}$ , and  $^{210}\text{Po}$ . The solid line denotes the PPC distribution, the dot-dashed denotes the Gaussian distribution. The Gaussian distributions are calculated with the same rms value  $\sigma = 20$ (a);  $20$ (b);  $24$ (c);  $24$ (d) keV (to reproduce the spreading widths of the IVGDR in accordance with the PPC results).

generated following the GOE distribution. This is discussed in Sec. IV C.

The coupling,  $V$ , between the doorway (one-phonon) states  $|d; \omega_i\rangle$ , and the background states,  $|b; \Omega_j\rangle$  is taken as

$$V = \sum_{i,k} V_{d_i, b_k} (Q_i^+ a_k + Q_i a_k^+), \quad (22)$$

with

$$V_{d_i, b_k} = \langle d; \omega_i | V | b; \Omega_k \rangle. \quad (23)$$

Notice that there is no coupling between individual one-phonon states, and no coupling between the background states. In the PPC model the matrix elements are microscopically obtained from Eq. (6). With the motivation above, we assume that these coupling matrix elements can be replaced by a random interaction where the matrix elements  $V_{d_i, b_k}$  are Gaussian distributed random numbers,

$$P(V_{d_i, b_k}) = \frac{1}{\sigma \sqrt{2\pi}} \exp\left(-\frac{V_{d_i, b_k}^2}{2\sigma^2}\right), \quad (24)$$

with the width or strength

$$\sigma = \sqrt{\langle V_{d_i, b_k}^2 \rangle}, \quad (25)$$

and fulfilling

$$V_{d_i, b_k} = V_{b_k, d_i}. \quad (26)$$

At this point a few comments are in order. This assumption is well justified due to the following reasons. In our microscopic model the distribution of *all* the phonon-phonon coupling matrix elements (the PPC) is well reproduced by a (truncated) Cauchy distribution. However, it was shown in Refs. [31,33] that the PPC matrix elements, following a Gaussian distribution (see Figs. 5) or a truncated Cauchy distributions (see Fig. 6), produce the same final spreading of the  $B(E1)$  strength in the doorway model, providing the rms-value of the matrix elements are the same. More importantly is the fact, that with this rms-value  $\sigma$ , the chaotic properties of the spectra are exhibited in NNSD and  $\Delta_3(L)$  statistics (see Figs. 3 and 4). To elucidate the chaotic properties of the spectrum we determine the best fit of the distribution  $P(s)$  in

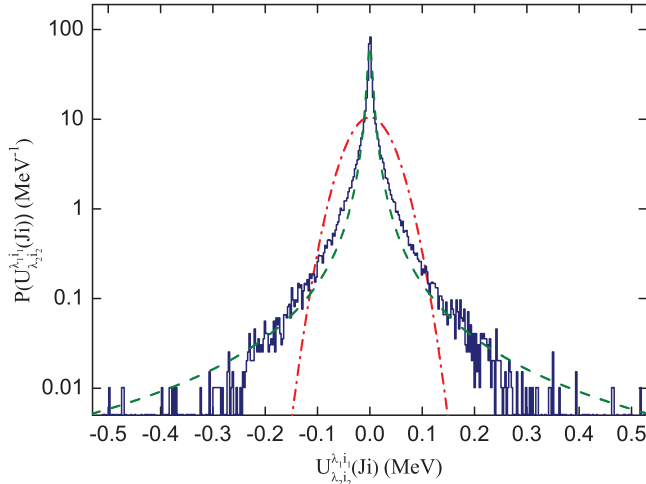


FIG. 6. Similar to Fig. 5, for the distribution obtained within RPA in case of  $^{206}\text{Pb}$ . The dashed line denotes the truncated Cauchy distribution. The Cauchy and Gaussian distributions are calculated with the same rms value  $\sigma = 38$  keV.

terms of the parameter  $q$ , to the Brody mixing function [4],

$$f(s; q) = \mathcal{A}(q + 1)s^q \exp(-\mathcal{A}s^{q+1}), \quad (27)$$

where

$$\mathcal{A} = \left[ \Gamma\left(\frac{q+2}{q+1}\right) \right]^{q+1}. \quad (28)$$

The limits  $q = 0$  and  $q = 1$  imply the Poisson and the GOE statistics, respectively. In particular, in case of  $^{208}\text{Pb}$  we obtain for the PPC results the value  $q \approx 0.2$  for the NNSD. Once we use the rms-value  $\sigma$  obtained from the truncated Cauchy distribution, and construct the final spectrum by means of the random coupling Eq. (24), the Brody mixing function yields the value  $q \approx 0.9$ . In other words, with the aid of this recipe we mimic the coupling of the one-phonon states with higher complexity configurations (i.e., the onset of the randomization).

At this stage we are ready to discuss the wave functions of the doorway model. Solving the eigenvalue problem for the total doorway Hamiltonian, Eq. (17), by a numerical diagonalization,

$$H|\mu\rangle = E_\mu|\mu\rangle, \quad (29)$$

one obtains the total wave functions as a mixture between the one-phonon states and background states,

$$|\mu\rangle = \sum_{i=1}^{N_d} c_i^\mu |d; \omega_i\rangle + \sum_{k=N_d+1}^N c_k^\mu |b; \Omega_k\rangle. \quad (30)$$

Such wave functions yield a fragmentation of the GDR strength on all  $N$  states, where  $N = N_b + N_d$  is the total number of states considered in the model. If there is no interaction between the one-phonon states and the background states ( $\sigma = 0$ ), the dipole strength distribution is concentrated on the one-phonon states. With the introduced coupling, the strength is spread over all  $\mu = 1 \dots N$  states with matrix

elements given by

$$P_\mu = \langle \mu | \mathcal{M}_{1-} | 0 \rangle = \sum_{i=1}^{N_d} c_i^\mu B_i, \quad (31)$$

where Eqs. (19) and (21) are used. The dipole matrix elements are thus distributed over the energy scale as

$$P(E) = \sum_{\mu=1}^N P_\mu \delta(E - E_\mu), \quad (32)$$

and the total dipole strength distribution becomes

$$b(E_1; E) = \sum_{\mu=1}^N |P_\mu|^2 \delta(E - E_\mu). \quad (33)$$

Subsequently, the photoabsorption cross section is obtained as

$$\sigma_{\text{abs}}(E) = \frac{16\pi^3}{3} \sum_{\mu=1}^N E |P_\mu|^2 \delta(E - E_\mu). \quad (34)$$

The total dipole strength distribution and the photoabsorption cross section distribution are finally averaged over many realisations of the random interaction (ensemble averaging). Usually the result is presented with a Lorentzian smoothing of the  $\delta$  functions.

Results for the nuclei  $^{206}\text{Pb}$  and  $^{206}\text{Hg}$ , based on the random matrix model with the assumption 1 for the background states, are shown in Figs. 2 and 7 for the photoabsorption cross-section distribution and the dipole strength distribution, respectively. Although the random distribution provides less details of fragmentation in the considered cases, the RMT approach yields the decay width values that are in a good agreement with the PPC results (cf. Table I).

It is noteworthy that the inclusion of the pairing forces does not affect the dipole strength distribution (compare the QRPA and RPA results in Fig. 7). This behavior can be understood from the following arguments. Assume that the two-phonon states have a constant level spacing  $d$ . For example, for the QRPA results we have  $d \approx 2.5$  keV, while for the RPA case  $d \approx 7.9$  keV. The strength function, calculated in the limit  $N \rightarrow \infty$  as the average over the distribution of the coupling matrix elements, is defined as (see Ref. [16])

$$\overline{b(E)} = \frac{1}{2\pi} \frac{\Gamma^\downarrow}{(E - E_c)^2 + (1/4)(\Gamma^\downarrow)^2}. \quad (35)$$

The average strength function (normalized to unity) has Lorentzian shape, while the spreading width is  $\Gamma^\downarrow = 2\pi\sigma^2/d$ . Evidently, the density of states and the strength of coupling matrix elements are changed due to the pairing [cf. Figs. 5(b) and 6]. However, the ratio  $\sigma^2/d$  remains approximately the same, and this explains the results displayed on Fig. 7.

## B. Determination of the coupling constant

The variable  $\sigma$  [Eq. (25)] determines the coupling strength between the one- and two-phonon (background) states. It can be obtained from the PPC calculations as the rms-value of the coupling matrix elements given by Eq. (6). We denote this microscopically determined strength value as  $\sigma_c$ .

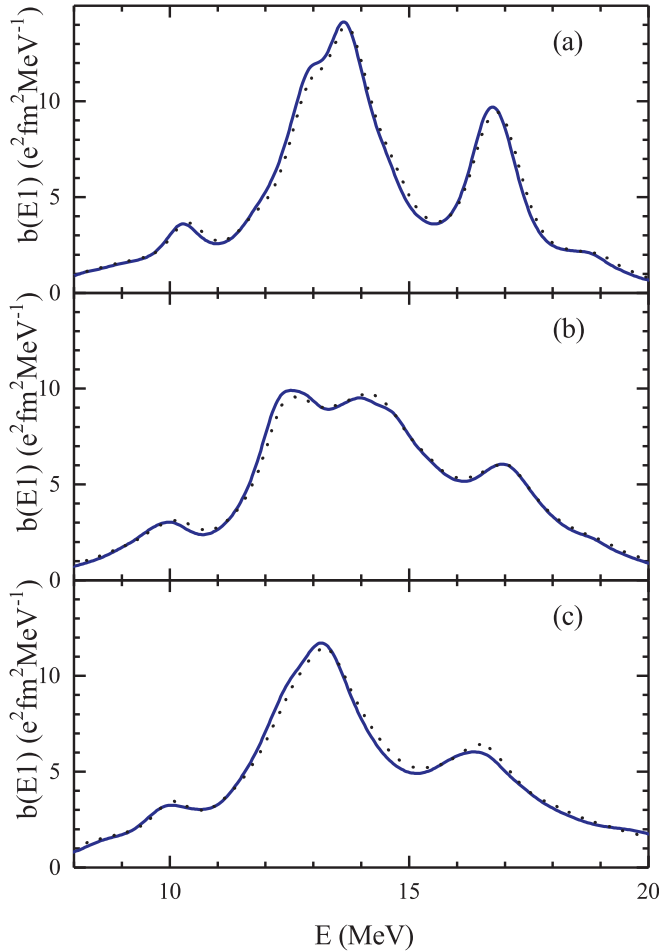


FIG. 7. Comparison of the results for the dipole strength distribution of  $^{206}\text{Pb}$ , obtained by means of: (a) the one-phonon approximation; (b) the PPC approach; (c) the random coupling matrix elements between the one- and two-phonon configurations. The solid and dotted lines correspond to the calculations within the RPA and the QRPA, respectively. The smoothing parameter 1 MeV is used for the strength distribution described by the Lorentzian function.

If the variable  $\sigma$  is treated as a parameter, one may study how the chaotic properties of the spectrum emerge as a function of the coupling strength in the following way. First, the energy spectrum  $\{E\}_N$  is obtained by means of the eigenvalue problem, Eq. (29), for a given parameter value. Next, with the aid of the unfolding procedure, we construct the NNSD, i.e., the distribution  $P(s)$  (see for details Ref. [61]).

We observe that with an increasing value of the variable  $\sigma$  the spectrum becomes increasingly chaotic (see Fig. 8). The exact value  $q = 1$  is difficult to obtain in the numerical simulations. Therefore, we consider chaos to appear at  $q \approx 0.95$ . It is quite astonishing that the strength  $\sigma_{\text{rand}}$ , that implies the onset of chaos, is approximately equal to  $\sigma_{\text{rand}} \approx \sigma_c$ , i.e., to the coupling strength obtained in the microscopic calculations. Consequently, without performing the full microscopic calculations of the coupling matrix elements, the coupling strength,  $\sigma_c$  can be approximately obtained from the value where chaos sets in.

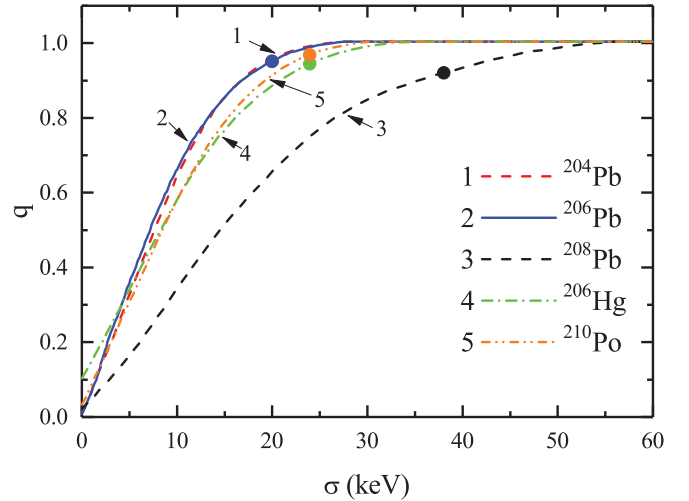


FIG. 8. The Brody mixing parameter,  $q$  versus the coupling strength,  $\sigma$ , for eigenenergies of the Hamiltonian Eq. (17) [see also Eq. (29)]. The different curves show the transition to the GOE statistics with  $q \rightarrow 1$ . The PPC values  $\sigma_c$  are indicated by circles on the corresponding curves.

### C. GOE-generated two-phonon energies

As was mentioned in Sec. IV A the energies of the background states may be obtained in another way than as the sum of two microscopically calculated phonon energies. We thus construct an energy stretch fulfilling GOE-statistics, and then unfold to energies with the same density of states as for two-phonon energies.

The staircase function  $N(E)$  of the two-phonon energies can be described by the following level density:

$$\rho(E) \propto (E - E_0)^\beta. \quad (36)$$

The staircase function of two-phonon  $1^-$  energies for  $^{206}\text{Pb}$  calculated with RPA and QRPA is shown in Fig. 9. We find that  $\beta = 2.64(3.31)$  for the QRPA(RPA) calculations. Notice that in the Fermi-gas model with equidistant single-particle states the exponent is  $2n - 1$  for the density of np-nh excitations, and the value  $\beta = 3$  for 2p-2h excitations, which is quite close to the fitted values of  $\beta$ .

The GOE spectrum is now generated with the aid of the GOE matrix, unfolded to have average energy distance equal to one, and then folded again with the level density given by Eq. (36). This procedure yields the energy spectrum with all GOE properties, and characterized by the level density  $\rho(E)$ . In the doorway model these energies are then used as the background energies,  $\{\Omega\}_{N_b}$  [Eq. (20)].

The comparison of the  $B(E1)$  strength distribution of  $^{206}\text{Pb}$ , obtained by means of the coupling between one-phonon states with two-phonon states that are: (i) the GOE generated; (ii) calculated microscopically, – is shown in Fig. 10. There is a remarkable agreement between the results for the cases (i) and (ii). Thus, we have formulated the model to obtain the fragmentation of the  $E1$  strength, that operates only the QRPA calculated one-phonon states. These ideas can subsequently be extrapolated to couplings to more complex underlying

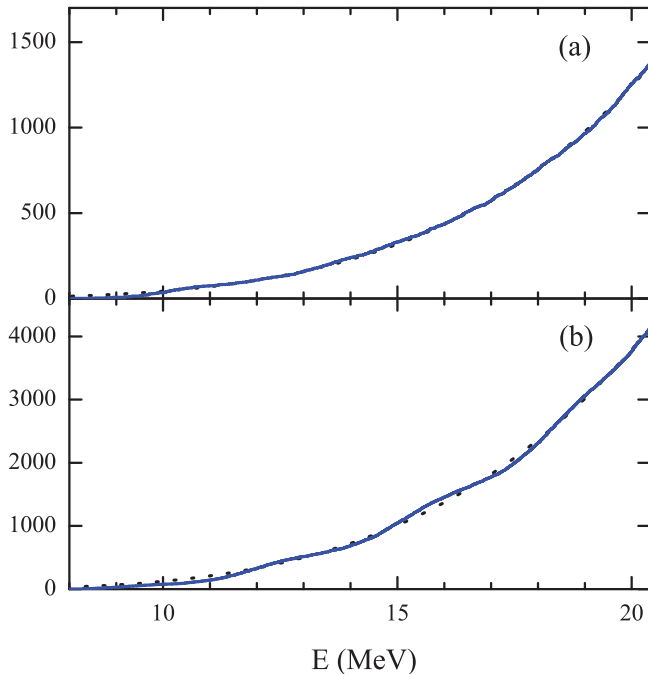


FIG. 9. The staircase function  $N(E)$  of the two-phonon  $1^-$  energies of  $^{206}\text{Pb}$ . The two-phonon energies (solid lines) are calculated within the RPA (top) and the QRPA (bottom). The dotted line denotes the  $N(E)$  function obtained with the level density.

states like 3-phonon states, 4-phonon states, etc., all with a quite easy computational efforts.

## V. SUMMARY

With the aid of the microscopic model based on the Skyrme interaction we have analyzed the strength distribution of  $1^-$  states in the region of the IVGDR, calculated for  $^{206}\text{Hg}$ ,  $^{204,206,208}\text{Pb}$ , and  $^{210}\text{Po}$  nuclei. To simulate the mean field we have used the SLy4 Skyrme interaction and the volume pairing interaction, treated in the BCS approximation. To analyze the  $1^-$  excitations we take into account all QRPA states with  $\lambda^\pi = 0^+, 1^-, 2^+, 3^-, 4^+$ . Within the QRPA approach the centroid location of the IVGDR is found at  $E \sim 14$  MeV for all considered nuclei. We have demonstrated that the PPC (the microscopic coupling) between the one- and two-phonon terms in the wave functions of excited states is important for the interpretation of the strength distribution of the IVGDR in the energy interval  $E_x \approx 9.5\text{--}18.5$  MeV. The results of the calculated transition-strength distribution are generally in a reasonable agreement with available experimental data. Based on this agreement we predict the characteristics of a few nuclei (see Table I), which might be a subject of experimental studies.

The obtained spectra are analyzed with the aid of the RMT correlation functions. Namely, the nearest-neighbour spacing distribution,  $\bar{\Delta}_3(L)$  statistics and the Porter-Thomas distribution, have been used to ascertain the chaotic properties of the IVGDR for the considered nuclei. The RMT measures related to the spectral properties display a weak transition towards the

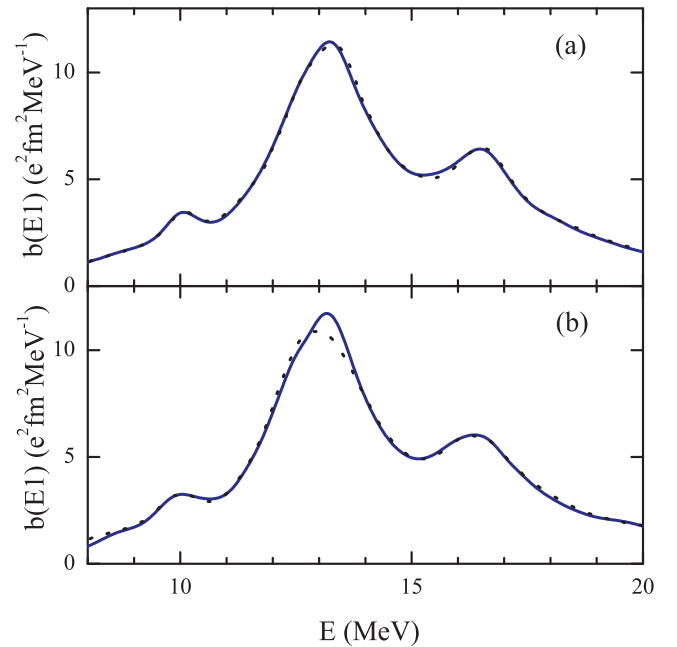


FIG. 10.  $B(E1)$  strength distribution of  $^{206}\text{Pb}$ : the comparison of the results obtained by means of the random coupling matrix elements between the one- and two-phonon configurations. Results of the calculations with the energies  $\omega_{\lambda_1 i_1} + \omega_{\lambda_2 i_2}$  (solid line) and with random GOE-generated two-phonon energies (dotted line) are shown. Both random strength distributions are obtained by ensemble averaging over 100 realisations. The one- and two-phonon energies are calculated within the RPA (top) and the QRPA (bottom). The smoothing parameter 1 MeV is used for the strength distribution described by the Lorentzian function.

GOE limit. We speculate that the inclusion of the coupling of the one-phonon states with higher complexity configurations could manifest much stronger degree of the randomization, i.e., the transition to the GOE limit. In fact, the results of the analysis of the probability  $B(E1)$  distribution demonstrate evidently the tendency to reach the Porter-Thomas limit, characteristic for the GOE statistics, indeed.

Guided by this analysis, we exploit further the ideas borrowed from the RMT: the coupling between one-phonon and two-phonon states is generated by means of the random distribution of coupling matrix elements Eq. (24). As a result, we have obtained a remarkable agreement on the spreading widths between the full microscopic calculations with the PPC and the random coupling, at the condition  $\sigma_{\text{rand}} \approx \sigma_c$ . The vitality of the obtained results enables us to extend the validity of our approach to the next level of simplifications. Namely, considering the microscopic one-phonon states coupled randomly to the two-phonons energies generated from the GOE distribution, we reproduce with a good accuracy the gross structure of decay widths obtained microscopically. It appears that this approach might simplify essentially the description of the IVGDR decay widths, at least, in heavy nuclei. Evidently, further systematic experiments would be helpful providing more precise data to test these theoretical ideas.

## ACKNOWLEDGMENTS

A.P.S. is grateful for the hospitality at the Division of Mathematical Physics, Lund University, where part of this work has been done. S.Å. thanks the Swedish Natural Science

Research Council for financial support and the Bogoliubov Laboratory of Theoretical Physics for warm hospitality. This work was partly supported by Russian Foundation for Basic Research under Grants No. 16-52-150003 and No. 16-02-00228.

- 
- [1] L. Muñoz, R. A. Molina, J. M. G. Gómez, and A. Heusler, *Phys. Rev. C* **95**, 014317 (2017).
- [2] B. Dietz, A. Heusler, K. H. Maier, A. Richter, and B. A. Brown, *Phys. Rev. Lett.* **118**, 012501 (2017).
- [3] M. L. Mehta, *Random Matrices*, 3rd ed. (Elsevier, Amsterdam, 2004).
- [4] T. A. Brody, J. Flores, J. B. French, P. A. Mello, A. Pandey, and S. S. M. Wong, *Rev. Mod. Phys.* **53**, 385 (1981).
- [5] S. Åberg, *Prog. Part. Nucl. Phys.* **28**, 11 (1992).
- [6] W. D. Heiss, R. G. Nazmitdinov, and S. Radu, *Phys. Rev. Lett.* **72**, 2351 (1994); *Phys. Rev. C* **52**, 1179(R) (1995); **52**, 3032 (1995); W. D. Heiss, R. A. Lynch, and R. G. Nazmitdinov, *ibid.* **60**, 034303 (1999).
- [7] V. Zelevinsky, B. A. Brown, N. Frazier, and M. Horoi, *Phys. Rep.* **276**, 85 (1996).
- [8] H. A. Weidenmüller and G. E. Mitchell, *Rev. Mod. Phys.* **81**, 539 (2009).
- [9] J. M. G. Gómez, K. Kar, V. K. B. Kota, R. A. Molina, A. Relaño, and J. Retamosa, *Phys. Rep.* **499**, 103 (2011).
- [10] M. N. Harakeh and A. van der Woude, *Giant Resonances: Fundamental High-Frequency Modes of Nuclear Excitation* (Clarendon Press, Oxford, 2001).
- [11] S. Adachi and N. Van Giai, *Phys. Lett. B* **149**, 447 (1984).
- [12] I. Hamamoto, H. Sagawa, and X. Z. Zhang, *Phys. Rev. C* **57**, 1064(R) (1998).
- [13] I. Poltoratska, R. W. Fearick, A. M. Krumbholz, E. Litvinova, H. Matsubara, P. von Neumann-Cosel, V. Y. Ponomarev, A. Richter, and A. Tamii, *Phys. Rev. C* **89**, 054322 (2014).
- [14] F. Knapp, N. Lo Iudice, P. Veselý, F. Andreozzi, G. De Gregorio, and A. Porrino, *Phys. Rev. C* **92**, 054315 (2015).
- [15] B. L. Berman and S. C. Fultz, *Rev. Mod. Phys.* **47**, 713 (1975).
- [16] A. Bohr and B. M. Mottelson, *Nuclear Structure* (Benjamin, New York, 1969), Vol. 1.
- [17] S. Åberg, *Phys. Rev. Lett.* **64**, 3119 (1990).
- [18] Ch. Stoyanov and V. Zelevinsky, *Phys. Rev. C* **70**, 014302 (2004).
- [19] N. Shimizu, T. Abe, M. Honma, T. Otsuka, Y. Tsunoda, Y. Utsuno, and T. Yoshida, *JPC Conf. Proc.* **6**, 010021 (2015).
- [20] R. Schwengner, R. Massarczyk, B. A. Brown, R. Beyer, F. Dönau, M. Erhard, E. Grosse, A. R. Junghans, K. Kosev, C. Nair, G. Rusev, K. D. Schilling, and A. Wagner, *Phys. Rev. C* **81**, 054315 (2010).
- [21] V. G. Soloviev, *Theory of Atomic Nuclei: Quasiparticles and Phonons* (Institute of Physics, Bristol and Philadelphia, 1992).
- [22] N. Van Giai, Ch. Stoyanov, and V. V. Voronov, *Phys. Rev. C* **57**, 1204 (1998).
- [23] A. P. Severyukhin, V. V. Voronov, and N. V. Giai, *Phys. Rev. C* **77**, 024322 (2008).
- [24] See discussion on self-consistent effects in various mesoscopic systems; for example, in J. L. Birman, R. G. Nazmitdinov, and V. I. Yukalov, *Phys. Rep.* **526**, 1 (2013).
- [25] C. W. J. Beenakker, *Rev. Mod. Phys.* **69**, 731 (1997).
- [26] W. D. Heiss and R. G. Nazmitdinov, *Physica D* **118**, 134 (1998).
- [27] Y. Alhassid, *Rev. Mod. Phys.* **72**, 895 (2000).
- [28] B. Lauritzen, P. F. Bortignon, R. A. Broglia, and V. G. Zelevinsky, *Phys. Rev. Lett.* **74**, 5190 (1995).
- [29] A. De Pace, A. Molinari, and H. A. Weidenmüller, *Nucl. Phys. A* **849**, 15 (2011).
- [30] W. D. Heiss, R. G. Nazmitdinov, and F. D. Smit, *Phys. Rev. C* **81**, 034604 (2010).
- [31] A. P. Severyukhin, S. Åberg, N. N. Arsenyev, and R. G. Nazmitdinov, *Phys. Rev. C* **95**, 061305(R) (2017).
- [32] V. Y. Ponomarev, *Phys. Rev. C* **97**, 059801 (2018).
- [33] A. P. Severyukhin, S. Åberg, N. N. Arsenyev, and R. G. Nazmitdinov, *Phys. Rev. C* **97**, 059802 (2018).
- [34] P. Ring and P. Schuck, *The Nuclear Many Body Problem* (Springer, Berlin, 1980).
- [35] J. P. Blaizot and D. Gogny, *Nucl. Phys. A* **284**, 429 (1977).
- [36] E. Chabanat, P. Bonche, P. Haensel, J. Meyer, and R. Schaeffer, *Nucl. Phys. A* **635**, 231 (1998) [Erratum: **643**, 441 (1998)].
- [37] P. Bonche, H. Flocard, P.-H. Heenen, S. J. Krieger, and M. S. Weiss, *Nucl. Phys. A* **443**, 39 (1985).
- [38] S. J. Krieger, P. Bonche, H. Flocard, P. Quentin, and M. S. Weiss, *Nucl. Phys. A* **517**, 275 (1990).
- [39] M. Wang, G. Audi, F. G. Kondev, W. J. Huang, S. Naimi, and X. Xu, *Chin. Phys. C* **41**, 030003 (2017).
- [40] J. Zenihiro, H. Sakaguchi, T. Murakami, M. Yosoi, Y. Yasuda, S. Terashima, Y. Iwao, H. Takeda, M. Itoh, H. P. Yoshida, and M. Uchida, *Phys. Rev. C* **82**, 044611 (2010).
- [41] A. P. Tonchev, N. Tsoneva, C. Bhatia, C. W. Arnold, S. Goriely, S. L. Hammond, J. H. Kelley, E. Kwan, H. Lenske, J. Piekarewicz, R. Raut, G. Rusev, T. Shizuma, and W. Tornow, *Phys. Lett. B* **773**, 20 (2017).
- [42] J. Piekarewicz, B. K. Agrawal, G. Colò, W. Nazarewicz, N. Paar, P.-G. Reinhard, X. Roca-Maza, and D. Vretenar, *Phys. Rev. C* **85**, 041302(R) (2012).
- [43] J. Terasaki, J. Engel, M. Bender, J. Dobaczewski, W. Nazarewicz, and M. Stoitsov, *Phys. Rev. C* **71**, 034310 (2005).
- [44] A. P. Severyukhin, V. V. Voronov, and N. Van Giai, *Eur. Phys. J. A* **22**, 397 (2004).
- [45] A. P. Severyukhin, N. N. Arsenyev, and N. Pietralla, *Phys. Rev. C* **86**, 024311 (2012).
- [46] M. Baldo, P. F. Bortignon, G. Colò, D. Rizzo, and L. Sciacchitano, *J. Phys. G* **42**, 085109 (2015).
- [47] G. Colò, P. F. Bortignon, N. Van Giai, A. Bracco, and R. A. Broglia, *Phys. Lett. B* **276**, 279 (1992).
- [48] M. Brenna, G. Colò, and P. F. Bortignon, *Phys. Rev. C* **85**, 014305 (2012).
- [49] V. V. Voronov and V. G. Soloviev, *Theor. Math. Phys.* **57**, 1001 (1983).
- [50] G. Baym and L. P. Kadanoff, *Phys. Rev.* **124**, 287 (1961).
- [51] E. Lipparini and S. Stringari, *Phys. Rep.* **175**, 103 (1989).
- [52] G. F. Bertsch, P. F. Bortignon, and R. A. Broglia, *Rev. Mod. Phys.* **55**, 287 (1983).

- [53] A. Avdeenkov, S. Goriely, S. Kamenzhiev, and S. Krewald, *Phys. Rev. C* **83**, 064316 (2011).
- [54] G. Scamps and D. Lacroix, *Phys. Rev. C* **88**, 044310 (2013).
- [55] E. Khan, N. Paar, D. Vretenar, Li-Gang Cao, H. Sagawa, and G. Colò, *Phys. Rev. C* **87**, 064311 (2013).
- [56] T. Oishi, M. Kortelainen, and N. Hinohara, *Phys. Rev. C* **93**, 034329 (2016).
- [57] R. R. Harvey, J. T. Caldwell, R. L. Bramblett, and S. C. Fultz, *Phys. Rev.* **136**, B126 (1964).
- [58] Yu. I. Sorokin, V. A. Khrushchev, and B. A. Yurev, *Bull. Acad. Sci. USSR, Phys. Ser.* **37**, 137 (1973).
- [59] N. Auerbach and A. Yeverehyahu, *Ann. Phys. (NY)* **95**, 35 (1975).
- [60] F. J. Dyson and M. L. Mehta, *J. Math. Phys.* **4**, 701 (1963).
- [61] A. P. Severyukhin, S. Åberg, N. N. Arsenyev, R. G. Nazmitdinov, and K. N. Pichugin, *Phys. At. Nucl.* **79**, 835 (2016).
- [62] O. Bohigas, M. J. Giannoni, and C. Schmit, *Phys. Rev. Lett.* **52**, 1 (1984).
- [63] A. Hamoudi, R. G. Nazmitdinov, E. Shahaliev, and Y. Alhassid, *Phys. Rev. C* **65**, 064311 (2002).
- [64] Y. Alhassid and M. Feingold, *Phys. Rev. A* **39**, 374 (1989).
- [65] Y. Alhassid and R. D. Levine, *Phys. Rev. Lett.* **57**, 2879 (1986).
- [66] C. E. Porter and R. G. Thomas, *Phys. Rev.* **104**, 483 (1956).